Journal of the Korean Chemical Society
2011, *Vol. 55, No. 3*
Printed in the Republic of Korea
DOI 10.5012/jkcs.2011.55.3.354

Iridium (III) quinoxaline 착물의 전자 구조, 인광 및 전기 발광 특성에 대한 DFT 및 시간-의존 DFT 연구

Xiao-Qing Zhou, Ying Li, Yan-Bo Sun*, and Hong-Xing Zhang
Institute of Theoretical Chemistry, State Key Laboratory of Theoretical and Computational Chemistry, Jilin University, Changchun 130023, People's Republic of China
(접수 2010. 11. 12; 수정 2011. 2. 5; 게재확정 2011. 3. 10)

DFT and Time-dependant DFT Investigation of eLectronic Structure, Phosphorescence and Electroluminescence Properties of Iridium (III) Quinoxaline Complexes

Xiao-Qing Zhou, Ying Li, Yan-Bo Sun*, and Hong-Xing Zhang
*Institute of Theoretical Chemistry, State Key Laboratory of Theoretical and Computational Chemistry, Jilin University, Changchun 130023, People's Republic of China. *E-mail address: syb@jlu.edu.cn*
(Received November 12, 2010; Revised February 5, 2011; Accepted March 10, 2011)

요 약. 3개의 적색 발광 Ir(III) 착물들인 $(fpmqx)_2Ir(L)$ {fpmqx=2-(4-fluorophenyl)-3-methyl-quinoxaline; L=triazolylpyridine (trz) (**1**); L=picolinate (pic) (**2**) and L=acetylacetonate (acac) (**3**)}의 전자 구조, 흡수 및 인광 메커니즘, 전기 발광(EL) 특성을 양자화학적으로 연구하였다. 계산 결과에 따르면, 1의 HOMO는 강한 ð-전자 받개 능력을 갖는 trz 부분에 편재되어 있으며, 2와 3의 HOMO는 Ir d-오비탈 과 페닐 고리 π-오비탈의 결합이라는 것을 나타내었다. 이 논문에서는 **1-3**사이의 인광 수득률과 차이에 대하여 연구하였으며, **1**과 **3**보다 **2**의 EL 효율이 더 큰 이유를 합리적으로 설명하였다.

주제어: 인광, 전기발광, 시간-의존 DFT 이론, 이리듐(III)

ABSTRACT. Quantum-chemistry study was explored to investigate the electronic structures, absorption and phosphorescence mechanism, as well as electroluminescence (EL) properties of three red-emitting Ir(III) complexes, $(fpmqx)_2Ir(L)$ {fpmqx=2-(4-fluorophenyl)-3-methyl-quinoxaline; L=triazolylpyridine (trz) (**1**); L=picolinate (pic) (**2**) and L=acetylacetonate (acac) (**3**)}. The calculated results show that the HOMO distribution for **1** is mainly localized on trz moiety due to its stronger π-electron acceptor ability, and HOMO for **2** and **3** is the combination of Ir d- and phenyl ring π-orbital. The higher phosphorescence yields and differences among **1-3** are investigated in this paper. In addition, the reasons of higher EL efficiency of **2** than **1** and **3** have been rationalized.

Keywords: Phosphorescence, Electroluminescence, Time-dependant DFT theory, Iridium (III)

INTRODUCTION

Organic light-emitting diodes (OLEDs) have attracted considerable attention for applications in multicolor displays and lighting applications.[1] In this field, phosphorescent Iridium (III) complexes are of paramount importance because of their high photoluminescence quantum yields and appropriate exciton lifetimes.[2] The strong spin-orbit coupling of heavy metal can effectively promote singlet-to-triplet intersystem crossing and enhance the subsequent radiative transition, which can to a large extent, partially remove the spin-forbidden nature from the triplet to the ground state. By using phosphorescent emitters in the active layer, it is possible to capture both singlet and triplet excited states and increase the internal quantum efficiency as high as 100%.[3] Among the three primary colors, however, the highly efficient pure-red-emitting complexes are still scarce[4] because of the low quantum yields result from a diminished HOMO-LUMO band gap, which facilitates the non-radiative process according to the energy gap rule.[5] Tuning phosphorescence wavelength and enhancing phosphorescent quantum yields in these complexes in a predictable way is a difficult task, and only red-emitting Ir (III) complexes show good efficiency/color purity trade-off can be used in the application in full-color flat-panel displays.

In conventional Ir (III) complexes containing simple C^N orthometalated ligands (such as phenylpyridine

(ppy)), theoretical investigations showed that the HOMO consists principally of a mixture of phenyl π- and Ir d-orbital, whereas LUMO is localized largely on the pyridyl π*-orbitals.[6] In this way, the modification of chelate ligand structure is an efficient way to tune the phosphorescence to longer wavelength, while changing the ancillary ligand leads only to a minor shift. Very recently, Johannes reported the red Ir (III) complexes containing 2-(4-fluorophenyl)-3-methyl-quinoxaline (fpmqx) as main cyclometalated and triazolylpyridine (trz), picolinate (pic), and acetylacetonate (acac) as ancillary ligands.[7] Compared with ppy, the increased π-electron accepting abilities and the extended π-conjugation length of fpmqx can significantly lower the LUMO energy levels for these complexes, therefore, changing ancillary ligands becomes the decisive structural factor for red color and efficiency determination of these Ir (III) complexes. In addition, fpmqx is more rigid than ppy ligand, which is beneficial for reducing non-radiative deactivation processes. It has been reported that the restricted intramolecular motion can suppress a non-radiative channel and result in enhanced phosphorescence in the solid state.[8]

In this paper, we carried out density functional theory (DFT) calculations of the above three Ir (III) complexes, aiming at providing an in-depth theoretical understanding of the higher phosphorescence quantum of these complexes arising from the fpmqx ligand. In addition, comparisons of electronic structure are made among **1-3** in an effort to rationalize the different function of ancillary ligands on phosphorescence quantum yields. This work provides a theoretical insight for the structure-driven tuning of the excited-state properties, thus open the way for future design and synthesis of new Ir (III) phosphors suited to higher performance PLEDs.

COMPUTATIONAL DETAILS

The ground-state and the lowest-lying triplet excited-state geometries were optimized by DFT[9] with Becke's LYP (B3LYP) exchange-correlation functional[10] and the configuration interaction with single excitations (CIS)[11] approach, respectively. There were no symmetry constraints on these complexes. At the respective optimized geometries of ground and excited states, TDDFT/B3LYP[12] calculations associating with the polarized continuum model (PCM)[13] in dichloromethane (CH_2Cl_2) media were carried out in order to obtain the vertical excitation energies of singlet (S_n) and triplet (T_n) states.

In the calculation, the quasi-relativistic pseudo-potentials of Ir atoms proposed by Hay and Wadt[14] with 17 valence electrons were employed, and a "double-ξ" quality basis set LANL2DZ was adopted. The selection of appropriate basis set for a given system is very important in ensuring high-quality results. However, the trade-off between accuracy and computational costs has to be weighted. Therefore, as an example, we optimized the geometry structure of **2** in the ground state with two sets of basis sets: LANL2DZ on all the atoms was used as BS1, LANL2DZ on Ir and 6-31G (d) on non-metal atoms was used as BS2. The calculated results are listed in *Table* 1. As shown, the more accurate results can be obtained from BS1. In BS2, the differences of Ir-C bonds and angles between two basis sets are negligible, while the Ir£¦N bonds are greatly overestimated by BS2. The calculated root-mean-square deviations of Ir-N bands for the structures optimized at two different basis set with respect to the experimental data are 2.8% and 3.9% for BS1 and BS2, respectively. Moreover, the calculation under BS1 level is more time-saving than BS2. Therefore, we adopted BS1 for all the calculations. Furthermore, the stable configurations of these complexes can be confirmed by frequency analysis, in which no imaginary frequency was found for these configurations at the energy minima. All calculations were performed with Gaussian 03 software package.[15]

RESULTS AND DISCUSSION

Geometries in the ground and the lowest lying triplet excited states

The sketch map for **1-3** is presented in *Scheme* 1 and the optimized ground-state structures are shown in *Fig.* 1 along with the numbering of some key atoms. The main structural parameters are summarized in *Table* 1 together with the X-ray crystal structures data of **2**.[7] The three complexes show a pseudo-octahedral coordination around the metal centers with the two N atoms residing at the *trans* location, and two carbon atoms at the *cis* location. *Table* 1 shows that the calculated bond lengths and bond angles are in good agreement with available crystal structural data,[7] and by changing ancillary ligands, three complexes show different bond lengths variation trend. For **1**, the calculated Ir-N3 bond is longer than Ir-N4, and Ir-C1 is shorter than Ir-C2. This can be rationalized by the presence of the ending phenyl ring on triazole moiety which can extend the π-electron delocalization between triazole and phenyl ring, and therefore, improve the cooperative effect.[1] The resulting effect is the elongation of Ir-C2 bond

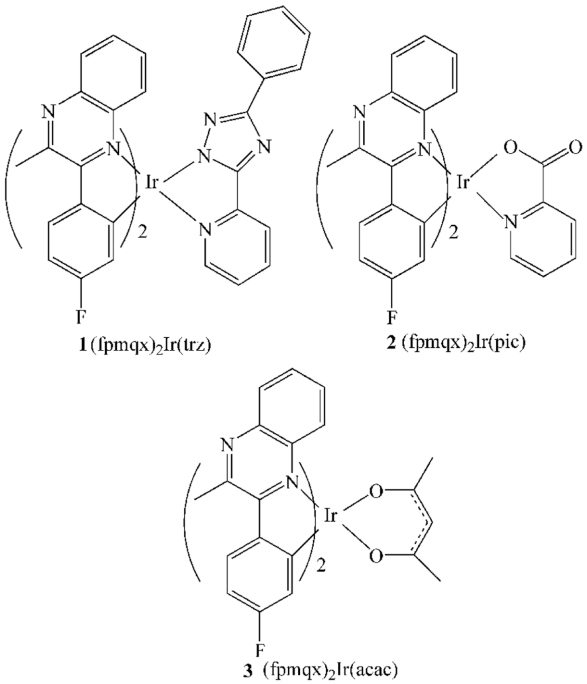

***Scheme* 1.** Sketch structures of three complexes.

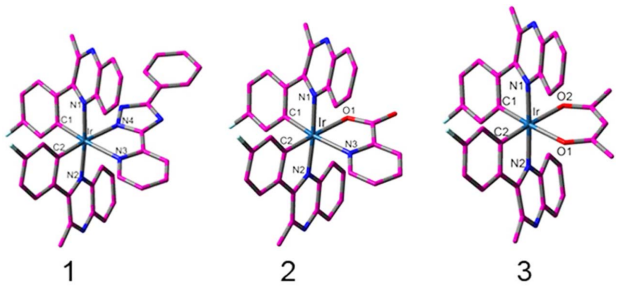

***Fig.* 1.** Optimized structures for **1-3** in the ground state at DFT/B3LYP level.

opposite to Ir-N4 bond. On the opposite, for **2**, the Ir-C1 bond is longer than Ir-C2, which can be ascribed to the stronger π-electron accepting ability of pyridine than COO^- group. For complex **3**, due to the same coordination condition, all the Ir-C or Ir-N bonds have the same values, respectively. Comparing with previously reported Ir (III) complexes,[17] most of the calculated bond lengths in this paper are shorter than those reported. This can be attributed to the presence of stronger π-electron accepting fpmqx ligand: the σ-electron donating properties of phenyl ring (ph), together with the stronger π-accepting ability of the quinoxaline (qux) fragment, may provide a synergism of electron delocalization so that the electron density is transferred from phenyl ring to the metal ion and back to the quinoxaline side, thus enhancing the chelate interaction.[18] This stronger metal-ligand interaction is significantly important to reduce the nonemissive transition channel and improve the phosphorescent quantum yields. Because the strengthened metal-ligand interaction is a critical factor to increase ^{3}MLCT character and therefore shorten the phosphorescence lifetime, which can partially remove the possibility of fast decay. In addition, the ligand with stronger interaction to metal can improve the thermal stability, and consequently extending the lifetime of OLED devices.

The calculated lowest triplet excited states geometrical parameters are also listed in *Table* 1. Comparing with the ground states, some Ir-N and Ir-C bonds elongate and some shorten in the excited states with respect to the ground state, but the differences are small. By careful analysis of the two fpmqx ligands, we found that they

***Table* 1.** Main optimized geometrical parameters for 1-3 at the B3LYP/LANL2DZ level together with the experimental data for 2 (the italic data in the second column are the geometrical parameters at the BS2 level for 2)

	1		**2**		**3**		Exptl [7]
	S_0	T_1	S_0	T_1	S_0	T_1	
			Bong length (Å)				
Ir-N1	2.099	2.123	2.093/*2.102*	2.113	2.076	2.075	2.062
Ir-N2	2.091	2.030	2.082/*2.094*	2.045	2.076	2.074	2.057
Ir-C1	2.005	2.007	2.005/*1.998*	2.003	1.991	1.981	1.985
Ir-C2	2.014	2.010	1.996/*1.993*	1.984	1.991	1.980	1.971
Ir-N3	2.248	2.264	2.200/*2.242*	2.217			
Ir-N4/O2	2.138	2.131			2.192	2.173	2.170
Ir-O1			2.190/*2.197*	2.177	2.192	2.173	2.156
			Bong angle (°)				
C1-Ir-N1	79.2	79.1	79.5/*79.3*	79.6	79.9	80.8	79.8
N1-Ir-N2	174.5	174.0	174.8/175.3	174.6	177.9	179.2	
			Dihedral angle (°)				
C1-Ir-N1-C2	91.2	90.7	91.4/	91.9	93.5	95.3	

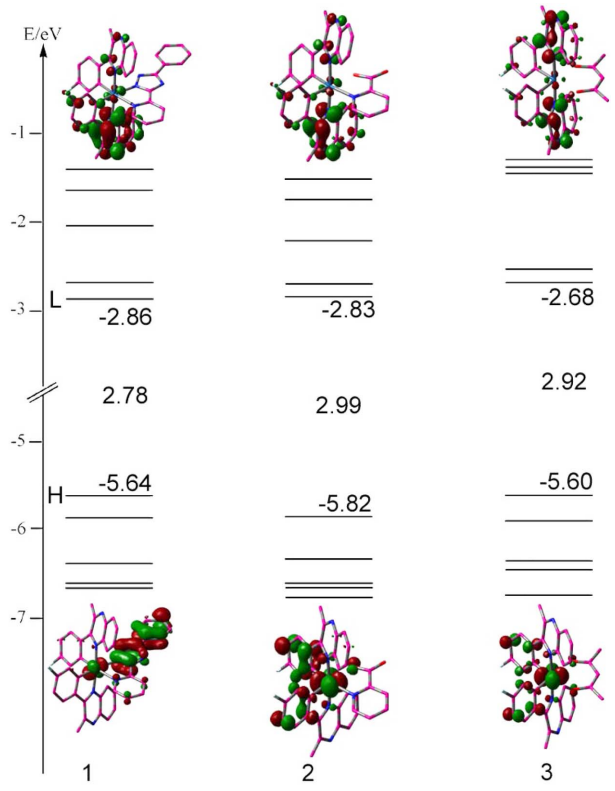

***Fig.* 2.** Presentation of partial orbital energy levels, energy gaps and orbital composition distribution for HOMO and LUMO for **1-3**.

have different elongation degree. This will result in the uneven electron density distribution on them. For **1** and **2**, one side of ancillary ligand is close to another side apart from the Ir atom, however, for **3**, metal-acac interaction became strengthened in T_1 state.

Froniter molecular orbital properties

The observed differences in the optical and chemical properties of complexes depend mainly on the changes of the ground-state electronic structure. Therefore, we will discuss in detail the HOMO and LUMO distribution and energy levels. The orbital energy levels and plots of HOMO and LUMO are presented in *Fig.* 2. The frontier molecular orbital (FMO) compositions of **1-3** are given in *Tables* 2-4, respectively.[19] As shown in *Fig.* 2 and *Table* 2, for **1**, due to the stronger metal-trz interaction and the π-electron accepting ability of trz, the HOMO is mainly residing on the trz moiety with composition up to 75.9%. The Ir dπ-orbital is antibonding combination with trz with only 13.9% composition. The HOMO distribution for **2** and **3** is significantly different from that of **1**, which is composed of Ir dπ-orbital and the phenyl ring moiety of fpmqx ligand due to the less stronger Ir-pic and Ir-acac interaction compared with Ir-trz, and the contribution from ancillary ligands can be negligible. The LUMO of the three complexes are very similar, with predominant contribution residing on the qux moiety, and the remaining largely localized on phenyl ring. In addition, the associated e_g*-like orbitals are 5.92, 6.14 and 6.16 eV higher in energy than HOMO, which are recognized as LUMO +14, LUMO+12 and LUMO+11 for **1-3**, respectively. It is notable that such a large d-orbital splitting can efficiently reduce the metal-centered (MC) dd excited states. Details of other orbitals can be obtained from *Tables* 2-4.

Moreover, the relative orbital energy levels are closely related to the photochemistry and electrochemistry properties. The concept of emission color tuning by variation of different ancillary ligand relies on the fact that the lowest excited state is relatively well described as a HOMO to LUMO transition in a given ligand.[20] *Fig.* 2 shows that complexes with different ancillary ligands have different HOMO and LUMO energy levels. The HOMO energy

***Table* 2.** Frontier molecular orbital composition (%) in the ground state for complex 1 at the B3LYP/LANL2DZ level (where H indicates the highest occupied molecular orbital (HOMO), and L indicates the lowest unoccupied molecular orbital (LUMO))

Orbital	Energy (eV)	MO composition (%)				Main bond type
		Ir	trz	ph	qux	
L+4	-1.43		59.1	9.6	30.8	π*(trz+qux)
L+3	-1.62		33.7	13.4	52.6	π*(trz+ph+qux)
L+2	-2.04	2.8	92.0	1.8	3.4	π*(trz)
L+1	-2.65	3.9	2.3	13.1	80.7	π*(ph+qux)
L	-2.86	4.3	2.3	16.7	76.7	π*(ph+qux)
H	-5.64	13.9	75.9	4.8	5.5	d(Ir)+π(trz)
H-1	-5.89	36.7	10.7	39.8	12.7	d(Ir)+π(trz+ph+qux)
H-2	-6.40	26.1	10.1	31.7	32.2	d(Ir)+π(trz+ph+qux)
H-3	-6.58	3.5	79.6	9.2	7.6	π(trz)
H-4	-6.65	23.8	25.1	23.9	27.2	d(Ir)+π(trz+ph+qux)
H-5	-6.70	29.1	5.4	32.0	33.5	d(Ir)+π(ph+qux)

***Table* 3.** Frontier molecular orbital composition (%) in the ground state for complex 2 at the B3LYP/LANL2DZ level (where H indicates the highest occupied molecular orbital (HOMO), and L indicates the lowest unoccupied molecular orbital (LUMO))

Orbital	Energy (eV)	MO composition (%)				Main bond type
		Ir	pic	ph	qux	
L+4	-1.50		20.4	17.5	61.7	π*(pic+ph+qux)
L+3	-1.74		74.7	5.3	19.3	π*(pic+qux)
L+2	-2.23	2.4	90.6	2.4	4.7	π*(pic)
L+1	-2.70	4.1	3.2	13.2	79.5	π*(ph+qux)
L	-2.83	4.6	2.3	16.7	76.3	π*(ph+qux)
H	-5.82	42.6	6.2	38.1	13.1	d(Ir)+π(ph+qux)
H-1	-6.30	39.7	18.9	14.8	26.6	d(Ir)+π(pic+ph+qux)
H-2	-6.56	7.8	18.7	42.3	31.2	π(pic+ph+qux)
H-3	-6.65	38.3	11.2	19.9	30.5	d(Ir)+π(pic+ph+qux)
H-4	-6.73		69.0	22.4	6.7	π(pic+ph)
H-5	-6.86	19.4	16.6	36.5	27.5	d(Ir)+π(pic+ph+qux)

***Table* 4.** Frontier molecular orbital composition (%) in the ground state for complex 3 at the B3LYP/LANL2DZ level (where H indicates the highest occupied molecular orbital (HOMO), and L indicates the lowest unoccupied molecular orbital (LUMO))

Orbital	Energy (eV)	MO composition (%)				Main bond type
		Ir	acac	ph	qux	
L+4	-1.30		10.4	15.7	73.3	π*(acac+ph+qux)
L+3	-1.39			19.4	80.0	π*(pic+qux)
L+2	-1.47	2.7	73.1	6.4	17.9	π*(acac+qux)
L+1	-2.51	6.3		11.9	80.5	π*(ph+qux)
L	-2.68	4.7		16.4	77.5	π*(ph+qux)
H	-5.60	43.9	6.0	37.4	12.6	d(Ir)+π(ph+qux)
H-1	-5.90	32.1	45.4	6.0	16.5	d(Ir)+π(acac+qux)
H-2	-6.35	1.6	11.4	48.9	38.1	π(acac+ph+qux)
H-3	-6.46	38.2	7.0	25.7	29.0	d(Ir)+π(ph+qux)
H-4	-6.72	12.1	25.5	33.7	28.6	d(Ir)+π(acac+ph+qux)
H-5	-6.74	31.1		34.8	32.1	d(Ir)+π(ph+qux)

level of **2** is much lower than **1** and **3**, which is not in consistent with the measured trend.[7] This can be rationalized by different conditions: in experiment, the measurement is influenced by many factors, such as temperature, solvent, and intermolecular π-π stacking, all of which can influence the HOMO energy levels as observed in previous theoretical reports.[21] The calculated LUMO energies are consistent with the experimental trend in the order **1**<**2**<**3**, and we noticed that the stronger π-electron accepting ability of ancillary ligand can lead to the lower LUMO energy. As expected, the calculated LUMO energies for **1-3** are much stabilized than other Ir(C^N)$_2$L complexes,[16] because of the stronger accepting ability of fpmqx ligand. Furthermore, the HOMO and HOMO-1, LUMO and LUMO+1 energy gaps are large for the three complexes. These large energy gaps demonstrate that HOMO to LUMO transition will be dominant in the lowest singlet and triplet transitions.

Absorption spectra

Starting from the ground-state geometries, the lowest singlet and triplet excited states were calculated by the TDDFT/B3LYP method with PCM in CH_2Cl_2 solution. The calculated absorption data are listed in *Table* 5. For clarity, only the most leading excited states (with larger CI coefficients) are listed. The fitted Gaussian type absorption curve is depicted in *Fig.* 3.

As shown in *Fig.* 3 and *Table* 5, the calculated lowest-energy absorption for **1-3** are at 541, 531 and 551 nm, respectively, which is consistent with the variation of HOMO-LUMO gaps, because the HOMO→LUMO transition configurations are predominantly $S_0 \rightarrow S_1$ transition. The intensity of $S_0 \rightarrow S_1$ transition for **1-3** can be negligible, which means that this transition is probably forbidden and would be practically absent in the absorption spectra. From the above discussion on FMO, the HOMO for **1** is mainly localized on the π-orbital of trz ligand and

***Table* 5.** Absorptions of 1-3 in CH_2Cl_2 solution according to TDDFT/B3LYP calculations

	States	λ(nm)/E(eV)	Oscillator	Main configurations	assign	exptl [7]
1	S_1	541/2.29	0.0093	H→L(86%)	d(Ir)+π(trz)→π*(ph+qux)/MLCT/LLCT	
				H-1→L(14%)	d(Ir)+π(trz+ph+qux)→π*(ph+qux)/MLCT/LLCT/ILCT	
	S_9	379/3.27	0.1371	H-3→L(79%)	π(trz)→π*(ph+qux)/LLCT	372
	S_{12}	361/3.44	0.0848	H-3→L+1(48%)	π(trz)→π*(ph+qux)/LLCT	361
				H-4→L+1(32%)	d(Ir)+π(trz+ph+qux)→π*(ph+qux)/MLCT/LLCT/ILCT	
	S_{13}	358/3.46	0.0882	H-6→L(67%)	d(Ir)+π(ph+qux)→π*(ph+qux)/MLCT/LLCT/ILCT	342
	S_{44}	283/4.38	0.0791	H-2→L+4(35%)	d(Ir)+π(trz+ph+qux)→π*(trz+qux)/MLCT/LLCT/ILCT	
				H-14→L+1	π(trz+ph)→π*(ph+qux)/LLCT/ILCT	
	S_{49}	275/4.50	0.3297	H→L+6(56%)	d(Ir)+π(trz)→π*(trz+ph)/MLCT/LLCT/ILCT	263
	S_{58}	267/4.64	0.1477	H-1→L+6(26%)	d(Ir)+π*(trz+ph+qux)π(trz+ph)/MLCT/LLCT/ILCT	
				H-8→L+2(25%)	π(trz)→π*(trz)/ILCT	
2	S_1	531/2.33	0.0078	H→L(100%)	d(Ir)+π(ph+qux)→π*(ph+qux)/MLCT/LLCT/ILCT	
	S_7	381/3.25	0.0669	H-3→L+1(49%)	d(Ir)+π(pic+ph+qux)→π*(ph+qux)/MLCT/LLCT/ILCT	
	S_8	378/3.28	0.1193	H-2→L(79%)	π(pic+ph+qux)→π*(ph+qux)/LLCT/ILCT	370
	S_{10}	356/3.48	0.0973	H-4→L(90%)	π(pic+ph)→π*(ph+qux)/LLCT/ILCT	
	S_{43}	277/4.48	0.1309	H→L+6(47%)	d(Ir)+π(ph+qux)→π*(ph)/MLCT/LLCT/ILCT	
	S_{54}	265/4.68	0.1009	H-4→L+3(52%)	π(pic+ph)→π*(pic+qux)/LLCT/ILCT	
	S_{55}	264/4.70	0.2359	H-2→L+5(55%)	π(pic+ph+qux)→π*(ph+qux)/LLCT/ILCT	256
3	S_1	551/2.25	0.0050	H→L(100%)	d(Ir)+π(ph+qux)→π*(ph+qux)/MLCT/LLCT/ILCT	
	S_3	496/2.50	0.0878	H-1→L(92%)	d(Ir)+π(acac+qux)→π*(ph+qux)/MLCT/LLCT/ILCT	
	S_7	383/3.23	0.0870	H-3→L(55%)	d(Ir)+π(ph+qux)→π*(ph+qux)/MLCT/LLCT/ILCT	371
				H-2→L+1(32%)	π(acac+ph+qux)→π*(ph+qux)/LLCT/ILCT	
	S_9	363/3.42	0.1340	H-4→L(98%)	d(Ir)+π(acac+ph+qux)→π*(ph+qux)/MLCT/LLCT/ILCT	
	S_{17}	337/3.68	0.1447	H-5→L+1(36%)	d(Ir)+π(ph+qux)→π*(ph+qux)/MLCT/LLCT/ILCT	346
	S_{37}	277/4.48	0.1613	H-12→L+1(32%)	d(Ir)+π(ph+acac)→π*(ph+qux)/MLCT/LLCT/ILCT	269
				H→L+5(22%)	d(Ir)+π(ph+qux)→π*(ph)/MLCT/LLCT/ILCT	
				H-3→L+3(22%)	d(Ir)+π(ph+qux)→π*(pic+qux)/MLCT/LLCT/ILCT	
	S_{40}	271/4.57	0.1472	H-2→L+4(40%)	π(acac+ph+qux)→π*(acac+ph+qux)/LLCT/ILCT	
	S_{43}	266/4.65	0.1561	H→L+7(40%)	d(Ir)+π(ph+qux)→π*(qux)/MLCT/LLCT/ILCT	255
				H-14→L(28%)	π(ph+qux)→π*(ph+qux)/LLCT/ILCT	

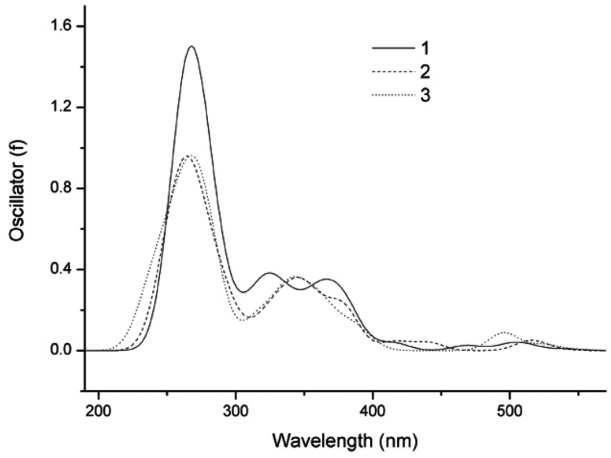

***Fig.* 3.** Simulated absorption spectra for **1-3** in CH_2Cl_2 media with data under TD-B3LYP level.

with small contribution from Ir dπ-orbital, and LUMO is π*-combination of ph and qux, therefore, the 541nm absorption for **1** can be described mainly as π(trz)→π*(ph+qux) transition with LLCT character, perturbed with some MLCT character [d(Ir)→π*(ph+qux)]. HOMO-1LUMO configuration also has some contribution to this 541 nm absorption [d(Ir)+π(trz+ph+qux)→π*(ph+qux)/MLCT/LLCT/ILCT]. For **2** and **3**, the 531 and 551 nm absorption are both composed of HOMO [d(Ir)+π(ph+qux)]→LUMO [π*(ph+qux)] transition with MLCT, LLCT and ILCT characters.

In experiment, the low intensity absorption in the region 450-600 nm do not appear in the singlet-to-singlet excited state calculation which indicates that it is triplet excited states. As shown in *Table* S1, these absorptions are consistent well with the triplet state absorption, and they can most be described as spin-forbidden ^{1}MLCT and ^{3}MLCT transition characters. The intensity of these triplet excited states is zero, because spin-orbital coupling (SOC) effect

is not included in the current TDDFT calculation. Su and his co-workers have calculated the Re(II) complexes with and without SOC effect, and showed that SOC has minor effect on the calculated excited energies.[22]

The first distinguishable absorption bands for **2** and **3** are localized at 370 and 371 nm, respectively, and this band for **1** splits into many shoulders at 372, 361 and 342 nm with the strongest at 372 nm, which is in consistent with the measured values.[7] For **1**, this 372 nm absorption is charge transfer (CT) transition from trz ligand to ph and qux moieties with LLCT characters. For the 370 nm absorption of **2**, in addition to the ancillary, the participation of ph and qux in donor orbital increased comparing with **1**. In **3**, the metal d-orbital also take part in the electron transition for the 371 nm absorption, which is in consistent with the weaker π-electron accepting ability of ancillary in the order **123**. The observed strongest absorptions are localized at 263, 256 and 269/255 nm for **1-3**, respectively. Our calculated results are 275, 264, 277/266 nm, slightly blue-shifted to higher energy region, and deviation from the measured values of about 12, 8, 8/11 nm, which is also consistent well with the experiment. The observed absorption band at 263 nm for **1** is mainly described by transition of HOMO→LUMO+6 and is assigned as trz-based LLCT transition, perturbed with some [d(Ir)→π*(trz+ph)]/MLCT characters. The 256 nm absorption band for **2** is contributed mainly by π(pic+ph+qux) π*(ph +qux) transition with LLCT and ILCT characters as shown in *Table* 5. For **3**, the 269 and 255 nm absorptions are composed by a series of very close transitions (277, 271 and 266nm) and they can be described as combination of MLCT, LLCT or ILCT transitions. In these high energy absorption bands, the calculated oscillator strength of **1** is significantly higher than **2** and **3**, which is proportional to transition moments. The transition moments reflect the transition probability from the ground state to the excited states. The higher transition probability to the excited states means the greater emission probability.[23] The transition moments for **1-3** are 1.7292, 1.4319 and 1.2123/1.1701 a.u., respectively. This means **1** has higher transition probability than **2** and **3**, which is important to enhance the phosphorescent quantum yields.

Electroluminescence (el) efficiency comparision in OLEDs

In experiment, complex **2** has the highest device efficiencies among the three complexes. To rationalize the reasons, the device configuration and energy levels for these complexes are shown in *Fig.* 4. As shown in *Fig.* 4, all the three complexes have higher HOMO energy levels than that of 4,4',4''-tris(N-carbazolyl)-triphenyl amine (TCTA)[24] (host material) (HOMO = 5.9eV), in addition, **1** and **2** have slightly lower HOMO energy than α-NPD (NPB, 4,4'-bis[N-(1-napthyl)-N-phenylamino]biphenyl, hole-transport layer) and **3** has higher HOMO energy than α-NPD. Therefore, hole can be easily injected from the HOMO of α-NPD to the HOMO of **1** and **2**, and hole can be injected directly from ITO electrode to its HOMO level for **3**. Due to the smaller HOMO energy gap between α-NPD and **2** (only 0.07 eV) than that between α-NPD and **1** (0.12 eV), hole injection efficiency into **2** is higher than **1**. However, for **3**, because there is no ladder between the HOMO of ITO electrode and **3**, the large energy gap of 0.84 eV leads to the lowest hole injection efficiency in **3** among the three complexes. In addition, due to the much lower HOMO energy level of 6.3 eV of TPBI, more hole will be accumulated on the HOMO of **2** than **1** and **3**. For LUMO energy levels, **1-3** all have the lower LUMO ener-

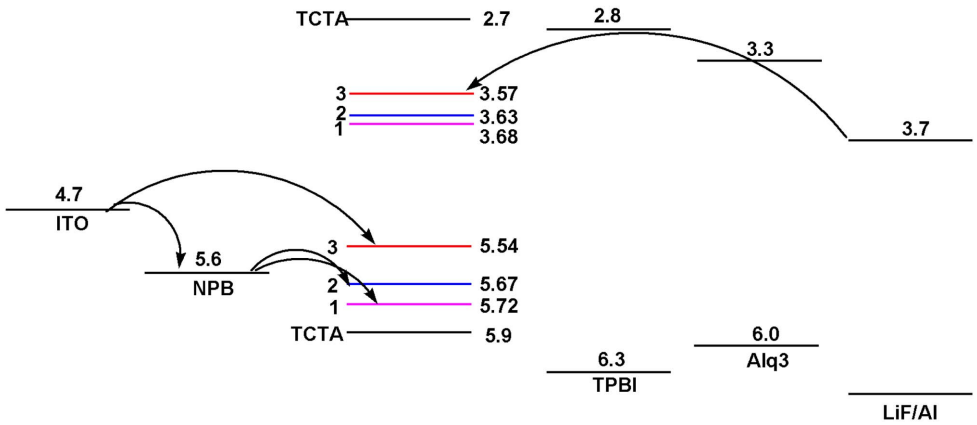

***Fig.* 4.** Energy levels of the materials used in the device fabrication, different colors indicate the HOMO and LUMO energy levels for **1-3**.

gies than that of 1,3,5-tri(phenyl-2-benzimidazole)-benzene (TPBI),[25] TCTA and Alq_3(trip(8-quinolinolato)-aluminum), and they are slightly higher than that of LiF/Al cathode of 3.7 eV. Thus, the electron trapping is the dominant EL mechanism as reported previously for many Eu^{3+} complexes.[26] Similarly, the small differences of LUMO energy gaps of 0.02 and 0.07 for **1** and **2** between LiF/Al cathode, respectively, make majority of electron will be accumulated in the LUMO of **1** and **2** than that of **3**. Therefore, recombination zone can be efficiently confined within the light-emitting layer for **1** and **2**, especially for **2**, which results in the highest device efficiency of 28019 cd/m^2 at 12.6 V for **2**.

Phosphorescence spectra

Based on the optimized geometrical structures under CIS method, the phosphorescence spectra for **1-3** were obtained in CH_2Cl_2 solution, and the results are listed in *Table* 6. The plots of molecular orbital related to emissions are presented in *Fig.* 5. The triplet excited state FMOs compositions are listed in *Table* S2 in supporting information.

The calculated phosphorescent emissions are localized at 719, 695 and 706 nm for **1-3**, respectively, corresponding to the experimental values of 605, 606 and 628 nm [7]. The calculated Stoke shifts between the lowest-lying triplet absorption and phosphorescence are 0.37, 0.33 and 0.29 eV for **1-3**, and the larger shifts are consistent with the structural relaxation in the excites states. For all the three complexes, each emission is composed of a series of transitions, and only the transition has the significant CI coefficients are listed in *Table* 6. As shown in *Table* 6, the 719 nm emission for **1** is mainly contributed by HOMO-2/-1LUMO transition configurations. *Table* S2 shows that the HOMO-2 is localized on the π-orbital of ph and qux moieties, and the Ir d-orbital increases in HOMO-1. LUMO resides predominantly on the qux moiety, with the remaining composition on the phenyl ring moiety, therefore, the 719 nm emission can be described as combination of [π(ph+qux)→π*(ph+qux)/^{3}LLCT/^{3}ILCT] and [d(Ir)+π(ph+qux)→π*(ph+qux)/^{3}MLCT/^{3}LLCT/^{3}ILCT] characters. The 695 nm emission for **2** has the similar transition characters, while the involving occupied orbitals are HOMO and HOMO-1. For **3**, the transitions are mainly ^{3}MLCT, ^{3}LLCT and ^{3}ILCT, and the participation of acac ligand appeared, due to its stronger interaction with metal

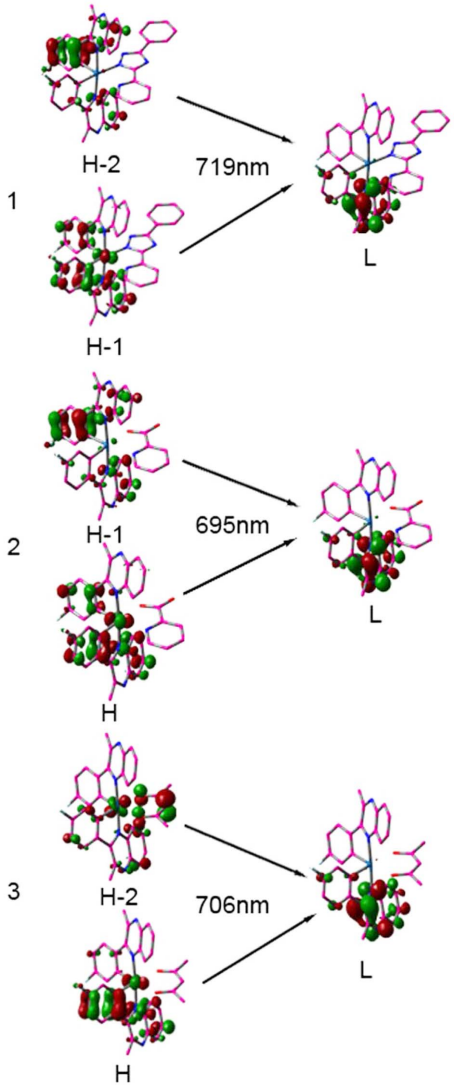

***Fig.* 5.** Singlet electron emission for **1-3**, calculated at TDDFT/B3LYP level in CH_2Cl_2 solution.

***Table* 6.** Calculated emission energies and dominant orbital emissions from TDDFT results for 1-3

		λ(nm)/E(eV)	Main configuration	assign	Exptl[7]
1	T_1	719/1.72	H-2→L (48%) H-1→L (41%)	π(ph+qux)→π*(ph+qux)/LLCT/ILCT d(Ir)+π(ph+qux)→π*(ph+qux)/MLCT/LLCT/ILCT	605
2	T_1	695/1.78	H-1→L (42%) H→L (32%)	π(ph+qux)→π*(ph+qux)/LLCT/ILCT d(Ir)+π(ph+qux)→π*(ph+qux)/MLCT/LLCT/ILCT	606
3	T_1	706/1.76	H→L (50%) H-2→L (38%)	d(Ir)+π(ph+qux)→π*(ph+qux)/MLCT/LLCT/ILCT d(Ir)+π(acac+ph+qux)→π*(ph+qux)/MLCT/LLCT/ILCT	628

***Table* 7.** Phosphorescence quantum yields (Φ), lifetime (τ), radiative decay rate (k_r) and nonradiative decay rate (k_{nr}) for 1-3

	Φ	τ	k_r ($\times10^{-5}s^{-1}$)	k_{nr} ($\times10^{-5}s^{-1}$)
1	0.42	2.6	1.6	2.2
2	0.39	2.1	1.9	2.9
3	0.41	1.7	2.4	3.5

Ir atom than those in **1** and **2**. In addition, we noted that for all the three complexes, there is a large contribution of ^{3}MLCT mixed with ligand-based $^3(\pi$-$\pi^*)$ transition. Our calculated results agree well with the experimental observations that the emission spectra are structureless,[7] because emission bands from ^{3}MLCT states are generally broad and featureless, while $^3(\pi$-$\pi^*)$ states typically give highly structured emission.[27]

From experimental data, we know that the three complexes with different ancillary ligands show slight differences in phosphorescent efficiencies. The k_r (radiative decay rate) and k_{nr} (nonradiative decay rate) were obtained according to $k_r=\Phi/\tau$ and $k_{nr}=(1-\Phi)/\tau$, where τ is the lifetime and Φ is the quantum yields, and the results are listed in *Table* 7. Previous reports shown that phosphorescent quantum efficiencies could be increased by a larger ^{3}MLCT composition, and consequently the $T_1\rightarrow S_0$ radiative transition can be increased, and hence shorten the radiative lifetime.[27] And it has been confirmed that ^{3}MLCT character controls the k_r value of the complexes.[28] And Zhang and co-workers have obtained similar conclusions according to TDDFT calculations of Ir(III) systems.[18] As shown in *Table* S2, the ^{3}MLCT composition can be obtained by MLCT%=M(occupied)%-M(unoccupied)%. Therefore, the calculated ^{3}MLCT characters for **1-3** are 10.4, 11.4 and 22.2%, respectively, which is consistent with the increased trend of k_r value for **1-3** in *Table* 7. For **2** and **3**, the slightly lower Φ value can be rationalized by the much large k_{nr} values. This can be ascribed to the more distorted triplet excited states structures, as shown in *Table* 1, which facilitates the nonradiative decay channels. Because Φ can be affected by the competition between k_r and k_{nr}, namely, $\Phi=k_r/(k_r+k_{nr})$. Therefore, to increase the quantum yield, k_r should be increased and k_{nr} should be decreased simultaneously or respectively.[29] Certainly, other factors, such as different temperature and environment can all resulting in different phosphorescent efficiencies among these complexes.

CONCLUSIONS

In this paper, geometrical, electronic structures, phosphorescence and electroluminescence properties of three Ir(III) complexes $(fpmqx)_2Ir(L)$ {fpmqx=2-(4-fluorophenyl)-3-methyl-quinoxaline; L=triazolylpyridine (trz) (**1**); L=picolinate (pic) (**2**) and L=acetylacetonate (acac) (**3**)} were investigated using DFT and TDDFT methods. The calculated results reveal that stronger π-electron accepting ability of trz than pic and acac can lead to HOMO distribution residing on trz moiety for **1**, and that for **2** and **3** are localized on Ir d- and phenyl ring π-orbital. The lowest energy absorption for **1-3** is mainly HOMOLUMO configuration, due to the large HOMO and HOMO-1, LUMO and LUMO+1 energy gaps, and all of them have mixed transition characters of MLCT, LLCT and ILCT. In addition, the higher electroluminescent efficiency of **2** than **1** and **3** comes from the relative smaller HOMO or LUMO energy differences between **2** and α-NPD and LiF/Al, which can improve the hole or electron injection efficiency and confine the recombination zone within the light-emitting layer.

REFERENCES

1. (a) D'Andrade, B. W. ; Forrest, S. R. *Adv Mater.* **2004**, *16*, 1585. (b) Ho, C. L.; Wang, Q.; Lam, C. S.; Wong, W. Y.; Ma, D.; Wang, L.; Gao, Z. Q.; Chen, C. H.; Cheah, K. W.; Lin, Z. *Chem Asian J.* **2009**, *4*, 89.
2. (a) Tsuboyama, A.; Iwawaki, H.; Furugori, M.; Mukaide, T.; Kamatani, J.; Igawa, S.; Moriyama, T.; Miura, S.; Takiguchi, T.; Okada, S.; Hoshino, M.; Ueno, K. *J Am Chem Soc.* **2003**, *125*, 12971. (b) Holmes, R. J.; Forrest, S. R.; Tung, Y. J.; Kwong, R. C.; Brown, J. J.; Garon, S.; Thompson, M. E. *Appl Phys Lett.* **2003**, *8*, 2422.
3. (a) Chou, P. T.; Chi, Y. Eur. J. *Inorg Chem.* **2006**, 3319. (b) Chou, P. T.; Chi, Y. *Chem Eur J.* **2007**, *13*, 380. (c) Burn, P. L.; Lo, S. C.; Samuel, I. D. W. *Adv Mater.* **2007**, *19*, 1675.
4. (a) Ho, C. L.; Wong, W. Y.; Gao, Z. Q.; Chen, C. H.; Cheah, K. W.; Yao, B.; Xie, Z.; Wang, Q.; Ma, D.; Wang, L.; Yu, X. M.; Kwok, H. S.; Lin, Z. *Adv Funct Mater.* **2008**, *18*, 319. (b) Liu, Z.; Guan, M.; Bian, Z.; Nie, D.; Gong, Z.; Li, Z.; Huang, C. *Adv Funct Mater.* **2006**, *16*, 1441. (c) Chen, X.; Liao, J. L.; Liang, Y.; Ahmed, M. O.; Tseng, H. E.; Chen, S. A. *J Am Chem Soc.* **2003**, *125*, 636.
5. (a) Cummings, S. D.; Eisenberg, R. *J Am Chem Soc.* **1996**, *118*, 1949. (b) Wilson, J. S.; Chawdhury, N.; Al-Mandhary, M. R. A.; Younus, M.; Khan, M. S.; Raithby, P. R.; Ko1hler, A.; Friend, R. H. *J Am Chem Soc.* **2001**, *123*, 9412.
6. Hay, P. J. *J Phys Chem A*. **2002**, *106*, 1634.
7. Schneidenbach, D.; Ammermann, S.; Debeaux, M.; Freund, A.; Zllner, M.; Daniliuc, C.; Jones, P. G.; Kowalsky, W.; Johannes, H.-H. *Inorg Chem*. **2010**, *49*, 397.
8. You, Y.; Huh, H. S.; Kim, K. S.; Lee, S. W.; Kim, D.;

Park, S. Y. *Chem Commun.* **2008**, 3998.
9. Runge, E.; Gross, E. K. U. *Phys Rew Lett.***1984**, *52*, 997.
10. Mayo, S. L.; Olafson, B. D.; Goddard, W. A. *J Phys Chem.* **1990**, *94*, 8897.
11. Foreman, J. B.; Gordon , M. H.; Pople, J. A. *J Phys Chem.* **1992**, *96*, 135.
12. (a) Helgaker, T.; Jrgensen, P. *J. Chem. Phys*. **1991**, *95*, 2595. (b) Bak, K. L.; Jdrgensen, P.; Helgaker, T.; Ruud, K.; Jensen, H. J. A. *J. Chem. Phys*. **1993**, *98*, 8873. (c) Autschbach, J.; Ziegler, T.; Gisbergen, S. J. A.; Baerends, E. J. *J. Chem. Phys.* **2002**, *116*, 6930.
13. Mennucci, B.; Tomasi, J. *J. Chem. Phys.* **1997**, *106*, 5151.
14. (a) Hay, P. J.; Wadt, W. R. *J. Chem Phys*. **1985**, *82*, 270. (b) Hay, P. J.; W. R. *J.Chem Phys.* **1985**, *82*, 299.
15. Frisch, M. J.; Trucks, G. W.; Schlegel, H. B.; Scuseria, G. E.; Robb, M. A.; Cheeseman, J. R.; Montgomery, J. A.; Vreven, Jr.T.; Kudin, K. N.; Burant, J. C.; Millam, J. M.; Iyengar, S. S.; Tomasi, J.; Barone, V.; Mennucci, B.; Cossi, M.; Scalmani, G.; Rega, N.; Petersson, G. A.; Nakatsuji, H.; Hada, M.; Ehara, M.; Toyota, K.; Fukuda, R.; Hasegawa, J.; Ishida, M.; Nakajima,T.; Honda, Y.; Kitao, O.; Nakai, H.; Klene, M.; Li, X.; Knox, J. E.; Hratchian, H. P.; Cross, J. B.; Adamo, C.; Jaramillo, J.; Gomperts, R.; Stratmann, R. E.; Yazyev, O.; Austin, A. J.; Cammi, R.; Pomelli, C.; J. Ochterski, W.; Ayala, P. Y.; Morokuma, K.; Voth, G. A.; Salvador, P.; Dannenberg, J. J.; Zakrzewski, V. G.; Dapprich, S.; Daniels, A. D.; Strain, M. C.; Farkas, O.; D. Malick, K.; A. Rabuck, D.; Raghavachari, K.; Foresman, J. B.; Ortiz, J. V.; Cui, Q.; Baboul, A. G.; Clifford, S.; Cioslowski, J.; Stefanov, B. B.; Liu, G.; Liashenko, A.; Piskorz, P.; Komaromi, I.; Martin, R. L.; Fox, D. J.; Keith, T.; Laham, M. A.; Peng, C. Y.; Nanayakkara, A.; Challacombe, M.; Gill, C. M. W.; Johnson, B.; Chen, W.; Wong, M. W.; Gonzalez, C.; and Pople, J. A. *Gaussian 03, revision C.02*; *Gaussion. Inc*.; *Wallingford CT.* **2004**.
16. Li, X. N.; Wu, Z. J.; Si, Z. J.; Zhang, H. J.; Zhou, L.; Liu, X. *J. Inorg Chem*. **2009**, *48*, 7740.
17. Li, X. N.; Wu, Z. J.; Zhang, H. J.; Liu, X. J.; Zhou, L.; Li, Z. F.; Si, Z. J. *Phys Chem Chem Phys.* **2009**, *11*, 6051.
18. Li, X. N.; Wu, Z. J.; Zhang, H. J.; Si, Z. J.; Zhou, L.; Liu, X. J. *Eur. J. Inorg Chem.* **2009**, 4052
19. Hu, X. Y.; Liu, X. J.; Feng, J. K. *Chinese. J. Chem.* **2007**, *25*, 1370.
20. Avilov, I.; Minoofar, P.; Cornil, J.; De Cola, L. *J Am Chem Soc.* **2007**, *129*, 8247.
21. Li, X. N.; Wu, Z. J.; Si, Z. J.; Zhou, L.; Liu, X. J.; Zhang, H. J. *Phys Chem Chem Phys.* **2009**, *11*, 9687.
22. Shi, L. L.; Liao, Y.; Zhao, L.; Su, Z. M.; Kan, Y. H.; Yang, G. C.; Yang, S. Y. *J Organomet Chem*. **2007**, *692*, 5368.
23. (a) Chu, T. Y.; Ho, M. H.; Chen, J. F.; Chen, C. H. *Chem Phys Lett.* **2005**, *415*, 137. (b) Tong, K. L.; So, S. K.; Ng, H. F.; Leung, L. M.; Yeung, M. Y.; Lo, C. F. *Synthe Met.* **2004**, *147*, 199. (c) Young, R. H.; Fitzgerald, J. J. *J Chem Phys.* **1995**, *102*, 2209.
24. Zhou, L.; Zhang, H. J.; Deng, R. P.; Guo, Z. Y.; Feng, J.; Li, Z. F. *J Phys Chem C*. **2008**, *112*, 15065.
25. Meyer, J.; Hamwi, S.; Bülow, T.; Johannes, H. H.; Riedl, T.; Kowalsky, W. *Appl Phys Lett.* **2007**, *91*, 113506.
26. Ying, L.; Zou, J. H.; Yang, W.; Zhang, A.; Wu, Z.; Zhao, W.; Cao, Y. *Dyes Pigments.* **2009**, *82*, 251.
27. Lamansky, S.; Djurovich, P.; Murphy, D.; Razzaq, F. A.; Lee, H. E.; Adachi, C.; Burrows, P. E.; Forrest, S. R.; Thompson, M. E. *J Am Chem Soc*. **2001**, *123*, 4304.
28. Haneder, S.; Da Como, E.; Feldmann, J.; Lupton, J. M.; Lennartz, C.; Erk, P.; Fuchs, E.; Molt, O.; Münster, I.; Schildknecht, C.; Wagenblast, G. *Adv Mater*. **2008**, *20*, 3325.
29. (a) Fantacci, S.; De Angelis, F.; Sgamellotti, A.; Marrone, A.; Re, N. *J Am Chem Soc*. **2005**, *127*, 14144. (b) Tamayo, A. B.; Garon, S.; Sajoto, T.; Djurovich, P. I.; Tsyba, I. M.; Bau, R.; Thompson, M. E. *Inorg Chem*. **2005**, *44*, 8723.

Journal of the Korean Chemical Society
2011, *Vol. 55, No. 3*
Printed in the Republic of Korea
DOI 10.5012/jkcs.2011.55.3.354

Iridium (III) quinoxaline 착물의 전자 구조, 인광 및 전기 발광 특성에 대한 DFT 및 시간-의존 DFT 연구

Xiao-Qing Zhou, Ying Li, Yan-Bo Sun*, and Hong-Xing Zhang

Institute of Theoretical Chemistry, State Key Laboratory of Theoretical and Computational Chemistry, Jilin University, Changchun 130023, People's Republic of China

Table S1. Triplet absorptions for 1-3 in CH_2Cl_2 solution at TDDFT/B3LYP level

	state	λ(nm)/E(eV)	Main configuration	assign	Exptl[7]
1	T_1	593/2.09	H-1→L+1(42%)	d(Ir)+π(trz+ph+qux)→π*(ph+qux)/MLCT/LLCT/ILCT	
			H→L+1(27%)	d(Ir)+π(trz)→π*(ph+qux)/MLCT/LLCT/ILCT	
	T_2	580/2.14	H→L+1(29%)	d(Ir)+π(trz)→π*(ph+qux)/MLCT/LLCT/ILCT	578
			H-2→L+1(27%)	d(Ir)+π(trz+ph+qux)→π*(ph+qux)/MLCT/LLCT/ILCT	
	T_3	538/2.30	H→L(55%)	d(Ir)+π(trz)→π*(ph+qux)/MLCT/LLCT/ILCT	539
	T_4	497/2.50	H-1→L+1(44%)	d(Ir)+π(trz+ph+qux)→π*(ph+qux)/MLCT/LLCT/ILCT	
			H-1→L(24%)	d(Ir)+π(trz+ph+qux)→π*(ph+qux)/MLCT/LLCT/ILCT	
	T_5	486/2.55	H→L+1(23%)	d(Ir)+π(trz)→π*(ph+qux)/MLCT/LLCT/ILCT	
	T_6	473/2.62	H-1→L+1(30%)	d(Ir)+π(trz+ph+qux)→π*(ph+qux)/MLCT/LLCT/ILCT	
			H→L+1(26%)	d(Ir)+π(trz)→π*(ph+qux)/MLCT/LLCT/ILCT	
	T_7	449/2.76	H→L+2(77%)	d(Ir)+π(trz)→π*(trz)/MLCT/ILCT	449
2	T_1	588/2.11	H→L(68%)	d(Ir)+π(ph+qux)→π*(ph+qux)/MLCT/LLCT/ILCT	
	T_2	579/2.14	H→L+1(55%)	d(Ir)+π(ph+qux)→π*(ph+qux)/MLCT/LLCT/ILCT	580
			H-1→L(21%)	d(Ir)+π(pic+ph+qux)→π*(ph+qux)/MLCT/LLCT/ILCT	
	T_3	517/2.40	H-1→L(40%)	d(Ir)+π(pic+ph+qux)→π*(ph+qux)/MLCT/LLCT/ILCT	
			H→L+1(23%)	d(Ir)+π(ph+qux)→π*(ph+qux)/MLCT/LLCT/ILCT	
	T_4	509/2.44	H-1→L+1(40%)	d(Ir)+π(pic+ph+qux)→π*(ph+qux)/MLCT/LLCT/ILCT	
	T_5	437/2.84	H-2→L+1(34%)	π(pic+ph+qux)→π*(ph+qux)/LLCT/ILCT	
			H-2→L(26%)	π(pic+ph+qux)→π*(ph+qux)/LLCT/ILCT	
3	T_1	606/2.05	H→L(84%)	d(Ir)+π(ph+qux)→π*(ph+qux)/MLCT/LLCT/ILCT	
	T_2	589/2.10	H→L+1(57%)	d(Ir)+π(ph+qux)→π*(ph+qux)/MLCT/LLCT/ILCT	592
			H-2→L(20%)	π(acac+ph+qux)→π*(ph+qux)/LLCT/ILCT	
	T_3	550/2.26	H-1→L(57%)	d(Ir)+π(acac+qux)→π*(ph+qux)/MLCT/LLCT/ILCT	547
			H→L+1(29%)	d(Ir)+π(ph+qux)→π*(ph+qux)/MLCT/LLCT/ILCT	
	T_4	523/2.37	H-1→L+1(38%)	d(Ir)+π(acac+qux)→π*(ph+qux)/MLCT/LLCT/ILCT	
			H-3→L(28%)	d(Ir)+π(ph+qux)→π*(ph+qux)/MLCT/LLCT/ILCT	
	T_5	471/2.63	H-2→L(37%)	π(acac+ph+qux)→π*(ph+qux)/LLCT/ILCT	
			H-1→L(26%)	d(Ir)+π(acac+qux)→π*(ph+qux)/MLCT/LLCT/ILCT	
			H-3→L+1(22%)	d(Ir)+π(ph+qux)→π*(ph+qux)/MLCT/LLCT/ILCT	
	T_6	456/2.72	H-1→L+1(56%)	d(Ir)+π(acac+qux)→π*(ph+qux)/MLCT/LLCT/ILCT	457
			H-3→L(25%)	d(Ir)+π(ph+qux)→π*(ph+qux)/MLCT/LLCT/ILCT	

Table S2. Frontier molecular orbital compositions (%) in T_1 state for 1-3 at CIS/LANL2DZ level

Complex	Orbital	Energy (eV)	Ir	MO composition			
				Trz/pic/acac	ph	qux	Main bond type
1	L	0.01	2.4	2.3	15.1	80.2	π*(ph+qux)
	H-1	-8.17	12.8/5.8 d_{yz} + 6.1 d_{xy}	1.1	44.0	42.1	d(Ir)+π(ph+qux)
	H-2	-8.38	2.4	1.6	45.9	50.2	π(ph+qux)
2	L	0.02	2.3	1.9	14.8	81.0	π*(ph+qux)
	H	-8.21	13.7/11.7 d_{xz}	1.2	43.8	41.3	d(Ir)+π(ph+qux)
	H-1	-8.42	3.1	0.6	42.8	53.5	π(ph+qux)
3	L	0.28	2.6	0.8	16.1	80.5	π*(ph+qux)
	H	-7.94	12.8/7.7 d_{z^2} + 2.8 $d_{x^2-y^2}$	0.9	43.4	42.9	d(Ir)+π(ph+qux)
	H-2	-8.74	14.6/8.9 d_{yz}	41.7	15.3	28.3	d(Ir)+π(acac+ph+qux)